iScience

CellPress
OPEN ACCESS

Article

# Renal inflammation combined with renal function reserve reduction accelerate kidney aging via pentose phosphate pathway

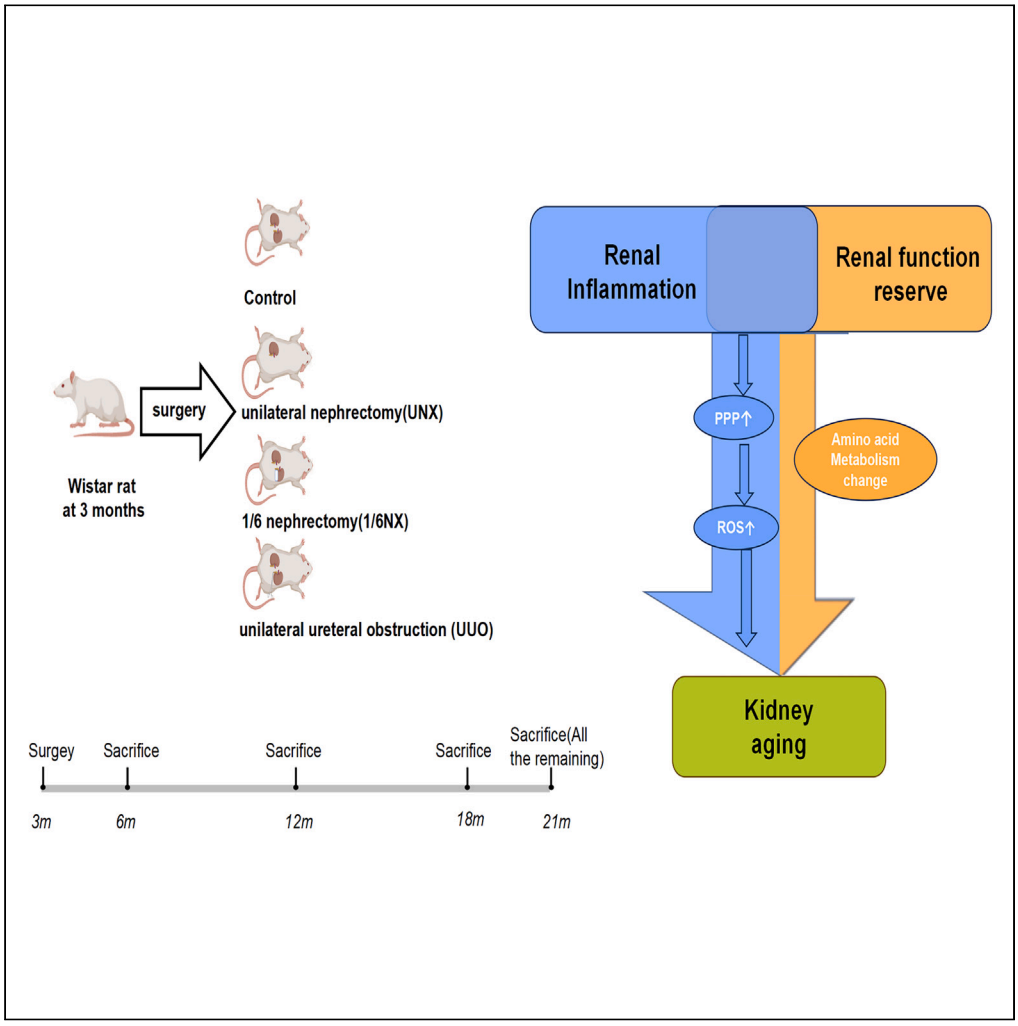


Bing Han, YiXuan Zhang, Chao Liu, ..., Guangyan Cai, Xiangmei Chen, Xuefeng Sun

xfssun@126.com

## Highlights

Renal inflammation and RFR decline can accelerate kidney aging

RFR decline may be associated with alterations in amino acid metabolism

PPP plays an important role in inflammation promoting aging

PPP can promote aging through oxidative stress

Han et al., iScience 27, 110045
June 21, 2024 
https://doi.org/10.1016/j.isci.2024.110045

iScience

CellPress
OPEN ACCESS

Article

# Renal inflammation combined with renal function reserve reduction accelerate kidney aging via pentose phosphate pathway

Bing Han,[1,4] YiXuan Zhang,[1,4] Chao Liu,[2] Pengcheng Ji,[1] Zenghui Xing,[1] Xiaodong Geng,[1] Kun Chi,[1] Ming Gong,[1] Yingying Li,[3] Ying Zhang,[3] Zhangning Fu,[1] Quan Hong,[1] Guangyan Cai,[1] Xiangmei Chen,[1] and Xuefeng Sun[1,5,*]

## SUMMARY

**Aging is closely associated with inflammation, which affects renal function reserve (RFR) in the kidneys. This study aims to investigate the impact of reduced RFR reduction on kidney aging and the influence of renal inflammation and RFR reduction on this process. Natural aging rats and those subjected to unilateral nephrectomy (UNX), 1/6 nephrectomy (1/6NX), and unilateral ureteral obstruction (UUO) were observed at 6, 12, 18, and 21 months. Our findings suggest that RFR reduction and renal inflammation can accelerate kidney aging, and inflammation contributes more. Metabolomics analysis revealed alterations in amino acid metabolism contribute to RFR decline. Furthermore, experiments *in vitro* confirmed the involvement of pentose phosphate pathway (PPP) in promoting aging though inflammation. Our research provides novel insights into for the mechanism of kidney aging and provides indirect support for clinical treatment decisions, such as addressing kidney inflammation, stones, or tumors that may necessitate partial or complete nephrectomy.**

## INTRODUCTION

Renal function reserve (RFR) is defined as the difference between the glomerular filtration rate (GFR) in the resting state and the maximum volume.[1] It is used to measure the kidney GFR in response to nephron compensation, increased renal blood flow, and ultrafiltration.[2] The aging kidney is characterized by glomerular and tubular hypertrophy, glomerulosclerosis, and tubulointerstitial fibrosis, which decrease renal blood flow and GFR, and reduces RFR.[3] Moreover, the number of functional glomeruli decreases with age due to the prevalence of arteriosclerosis, glomerulosclerosis, tubular atrophy with interstitial fibrosis, and compensatory hypertrophy of the remaining nephrons.[4] A clinicopathological study showed that an increase in glomerular volume can cause podocytes to fall off, which may lead to focal glomerulosclerosis and aggravate kidney aging.[5] However, there is no direct evidence that RFR reduction promotes renal aging.

Inflammation is a highly significant risk factor for driving the aging process and leads to fibrosis of tissues and organs.[6] Although 24% of older adults have decreased renal function, very few develop end-stage renal disease (ESRD), and inflammation can accelerate kidney aging and lead to renal dysfunction.[7]

What is the contribution of renal inflammation and RFR reduction to kidney aging? Can renal inflammation promote the process of RFR reduction affects kidney aging? At present, there is a lack of corresponding evidence. In this study, naturally aging rats were used as controls, unilateral nephrectomy (UNX), and 1/6 nephrectomy (1/6NX) were used to simulate different levels of RFR reduction in rats, and unilateral ureteral obstruction (UUO) was used to simulate the coexistence of renal inflammation and RFR reduction in rats. Take samples for testing at the 3, 9, 15, and 18 months after surgery, respectively, to explore the influence of RFR reduction and renal inflammation on kidney aging in the process of natural aging. Our research provides new ideas for understanding the mechanism of kidney aging and provides circumstantial evidence for clinical treatment decisions regarding kidney inflammation, stones or tumors that require partial or single nephrectomy.

[1]Department of Nephrology, First Medical Center of Chinese PLA General Hospital, Nephrology Institute of the Chinese People's Liberation Army, State Key Laboratory of Kidney Diseases, National Clinical Research Center for Kidney Diseases, Beijing Key Laboratory of Kidney Disease Research, Beijing 100853, China
[2]Department of Critical Care Medicine, First Medical Center of Chinese PLA General Hospital, Beijing 100853, China
[3]Department of Ultrasound, First Medical Center of Chinese PLA General Hospital, Beijing 100853, China
[4]These authors contributed equally
[5]Lead contact
*Correspondence: xfssun@126.com
https://doi.org/10.1016/j.isci.2024.110045

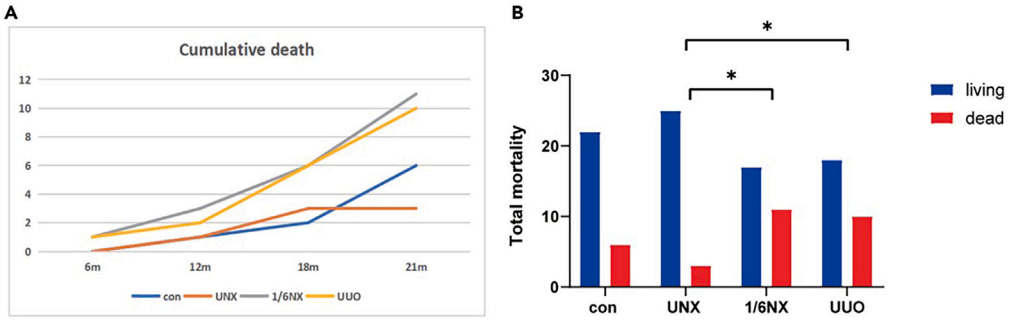


**Figure 1. The cumulative death and cumulative mortality of rats in each group ($n$ = 28)**

(A) The cumulative death of rats in each group. Y axis represents the total number of deaths.

(B) The total mortality of rats in each group. The mortality of UUO group and 1/6NX group was significantly higher than that of UNX group ($P < 0.05$).

## RESULTS

### Mortality of rats in each group

As shown in Figure 1, compared with-type wild rats, there was no significant difference in the total mortality rate of rats in the UNX group (21% and 10%). The total mortality of rats in the 1/6NX group increased the most significantly (39%), followed by that in the UUO group (36%). Total mortality in the UUO and 1/6NX groups was significantly higher than that in the UNX group.

### Kidney weight, renal size, and cortical thickness

Compared with that in wild-type rats, the kidney weight (KW)/body weight (BW) in the UUO group increased most obviously, followed by that in the UNX group. The KW/BW in 1/6NX the group did not change significantly (Figures 2D and 2E). Compared with those in wild-type rats, renal volume, and cortical thickness in the UUO group increased significantly at 12 months and lasted until 21 months. In the UNX group, renal volume began to increase significantly at 18 months, and cortical thickness increased significantly at 21 months. There was no significant difference in renal volume or cortical thickness between the 1/6NX rats and control groups (Figures 2B, 2C, 2F, and 2G). In short, the UUO group exhibited the most obvious compensatory effects on kidney mass and volume, followed by the UNX and 1/6 NX groups.

### Renal function of rats in each group

As shown in Figures 3A and 3B, compared with those of wild-type rats, creatinine levels in the UUO group increased significantly at 6 months, and this change lasted until 21 months. The creatinine level of rats in the UNX group increased significantly at 6 months, decreased at 12 months, increased again at 18 months, and contributed to increase until 21 months. Renal function in the 1/6NX group was compensated, and the level of creatinine did not increase significantly. Compared with those of wild-type rats, blood urea nitrogen (BUN) levels in the UUO group increased significantly at 12 months, decreased at 18 months and increased again at 21 months. BUN levels of rats in the UNX group increased significantly at 12 months, and then decreased (Figures 3C and 3D). In conclusion, levels of creatinine and BUN in the UUO group most obviously increased with age, followed by those in the UNX group, and the 1/6NX group did not exhibit obvious renal dysfunction.

### Renal fibrosis in each group

As shown in Figures 4A, 4B, 4D, and 4E, compared with those in wild-type rats, there was no significant change in the area of the area of renal fibrosis showed by Sirius red staining at 6 months. However, there was a significant increase in renal interstitial matrix indicated by PAS staining in the UUO and 1/6NX groups. At 12 months, renal fibrosis showed by PAS staining and Sirius red staining showed a significant increase in renal fibrosis in the UUO group. PAS staining in the UNX and 1/6NX groups revealed a notable increase in the area of renal fibrosis, although it was significantly lower than that in the UUO group. At 18 months, the rats in the UUO, UNX, and 1/6NX groups exhibited significant increase in renal fibrosis shown by in PAS staining and Sirius red staining. The UUO group was significantly higher than that in the UNX and 1/6NX groups. At 21 months, the area of renal interstitial matrix showed by PAS staining and the area of renal fibrosis showed by Sirius red staining increased significantly in the UUO and UNX groups. The UUO group had significantly higher levels compared to the UNX groups. Figures 4C and 4F displayed the changes in renal fibrosis with aging in each group using PAS and Sirius red staining. The UUO group showed the most pronounced progression of renal fibrosis during aging process, followed by the 1/6NX and UNX groups.

### Renal inflammation and ROS of rats in each group

The inflammatory makers IL-6, TNF-$\alpha$, and p-p65 were used to evaluate inflammation in the kidney of rats in each group. As shown in Figures 5A and 5B, compared with those of wild-type rats, inflammatory marker levels in the UUO, 1/6NX, and UNX groups increased

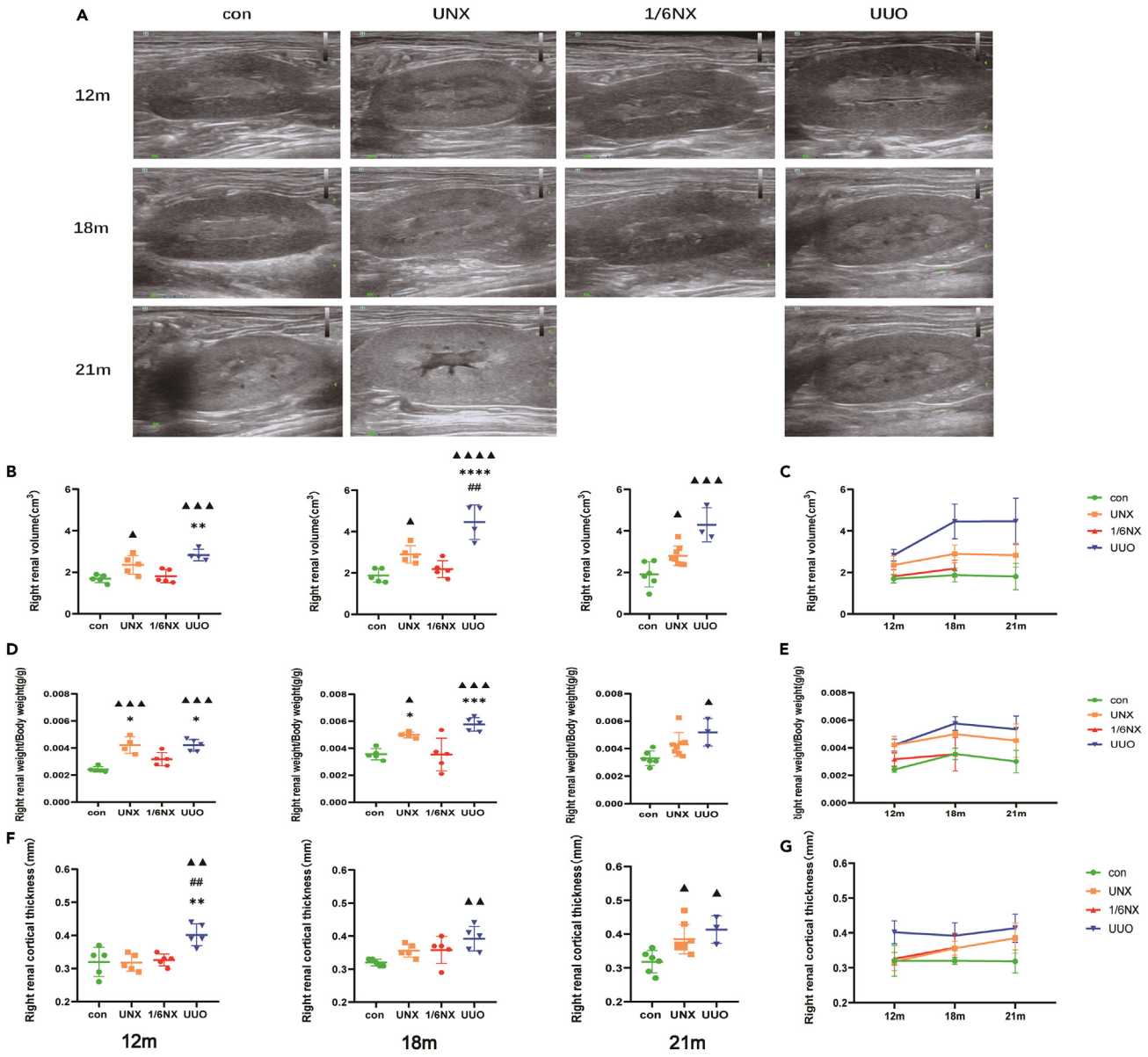


**Figure 2. Kidney weight, renal size, and cortical thickness (n = 3–8)**

(A) Renal ultrasound images of rats at the age of 12, 18, and 21 months in each group.

(B) Right renal volume at the age of 12, 18, and 21 months in each group.

(C) The trends of right renal volume at the age of 12, 18, and 21 months in each group.

(D) Renal weight/body weight at the age of 12, 18, and 21 months in each group.

(E) The trends of right renal weight/body weight of rats in each group with aging.

(F) Right cortical thickness at the age of 12, 18, and 21 months in each group.

(G)The trends of right cortical thickness of rats in each group with aging. Values are presented as means ± SD. ▲ $p < 0.05$, ▲▲ $p < 0.01$, ▲▲▲<0.001, ▲▲▲▲$p < 0.0001$ versus the control group, *$p < 0.05$, **$p < 0.01$, ***$p < 0.001$ versus 1/6NX group, ##$p < 0.01$ versus the UNX group.

significantly at 6–21 months. Rats in UUO group increased the most, followed by the 1/6NX group. In addition, a significant increase in reactive oxygen species (ROS) levels was observed in the UUO group compared to wilt-type rats at 6 months. Between 12 and 18 months, there was a significant increase in ROS levels in the 1/6NX and UUO groups, with the 1/6NX group displaying lower levels than the UUO group. The most pronounced increase was observed in the UUO group at 21 months, followed by the UNX group (Figures 5C and 5D). In conclusion, in the process of natural aging, the most severe inflammation and ROS in the kidneys was observed in the UUO group, followed by the 1/6NX and UNX groups.

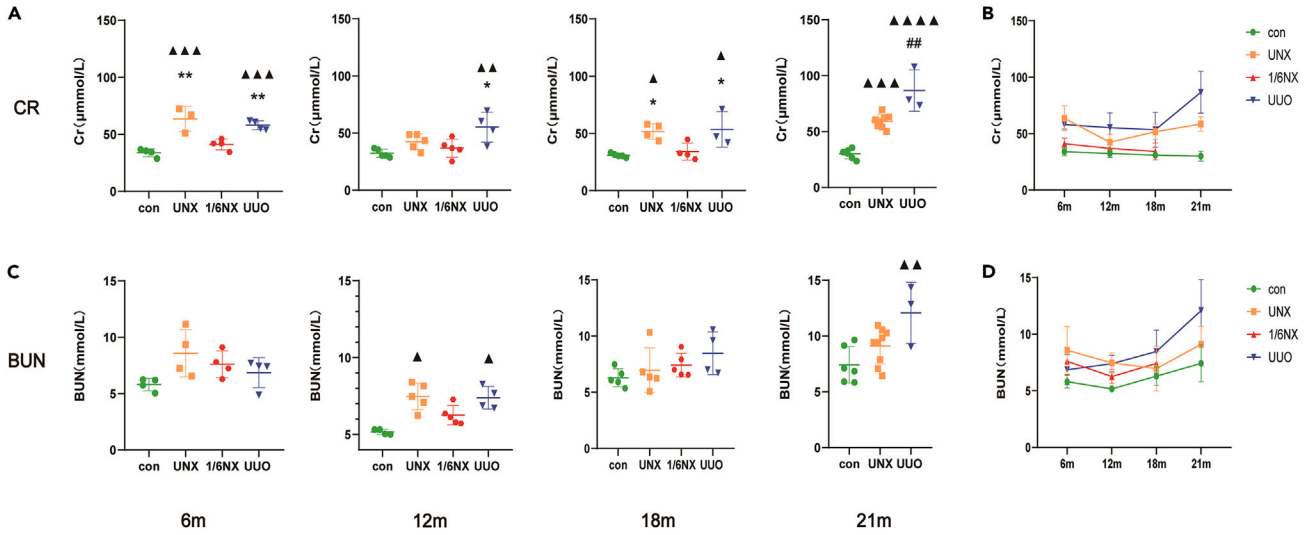


**Figure 3. Renal function of rats in each group (n = 3–9)**

Serum creatinine (A) and BUN (C) of rats at the age of 12,18 and 21 months in each group. The trends of Serum creatinine (B) and BUN (D) levels of rats in each group with aging. Values are presented as means ± SD. ▲ $p < 0.05$, ▲▲ $p < 0.01$, ▲▲▲ $<0.001$, ▲▲▲▲ $p < 0.0001$ versus the control group, *$p < 0.05$, **$p < 0.01$ versus 1/6NX group, ##$p < 0.01$ versus the UNX group.

## Renal aging of rats in each group

As depicted in Figures 6A and 6B, there were no significant differences in the expression of P16, P21, P53, and γH2AX among the rats in the different groups at 6 months. At 12 months, the UUO group showed a significant increase in γH2AX expression, followed by the 1/6NX group, with no change in the UNX group. And between 18 and 21 months, the UUO group exhibited significant increase in the express of P16, P21, P53, and γH2AX, followed by the 1/6NX and UNX groups. Besides, Figures 6C and 6D showed that there were no significant changes in the SA-β-gal content in rat tissues between 6 and 12 months across all groups. However, the UUO group exhibited a significant increase at 18–21 months. In the process of natural aging, rats in the UUO group displayed obvious premature aging, followed by the 1/6NX group, and finally the UNX group.

## Untargeted UPLC-MS/MS analysis

The quality of five duplicate samples in each group was analyzed, and the principal-component analysis (PCA) and Pearson's correlation coefficient analysis showed that the quality of the samples was suitable for subsequent analysis (Figures 7A–7C).

Partial least squares discriminant analysis (PLS-DA) was performed on the metabonomic data (Figures 8A–8C). By combining the PLS-DA results for the top 30 metabolites, raw $P < 0.05$, and the measurable mean ratio, we obtained the differentially abundant metabolites of kidney tissue in the UNX, 1/6NX, and UUO groups, as shown in Tables S3–S5. The changes in renal metabolism in the UNX group mainly involved amino acid metabolism, which was characterized by the accumulation of a variety of amino acid metabolites. There are also metabolic changes in lipids, nucleotides, cofactors, vitamins, xenobiotics, and peptides. In the 1/6NX group, there were obvious changes in glucose metabolism in the kidney, such as an increase in the glycolytic pathway and activation of the pentose phosphate pathway (PPP) and other glucose metabolism pathways; these changes involved decrease in glucose, galactose-1-phosphate, D-galactose-6-phosphate, 3-phosphoglycerate, phosphoenolpyruvate (PEP), 6-phosphogluconate, glucuronate 1-phosphate, and N-acetylglucosamine 6-phosphate. In the UUO group, there were also changes in glucose metabolism, including enhanced glycolysis and PPP activation: the level of 3-phosphoglycerate, 6-posophogluconate, sedoheptulose-7-phosphate and glucuronate-1-phosphate were increased, while the level of glycerate was decreased. Other metabolic changes include changes in amino acids , lipids, nucleotides, cofactors, vitamins, xenobiotics, and peptides. Through metabonomic analysis, we found that the changes in kidney metabolism in the UNX group were mainly associated with amino acids, which may be due to the loss of RFR. However, there were similar changes in glucose metabolism in the kidney in the 1/6NX and UUO groups; these changes involved an increase in the products of the PPP, indicating activation of the PPP. It has been found that inflammation upregulate the PPP and activate NADPH oxidase 2 (NOX2) to promote the oxidative stress response, further aggravating inflammatory.[8–10] Moreover, the accumulation of damage caused by ROS, such as superoxide anions, hydroxyl radicals, and hydrogen peroxide (H2O2), is an important factor promoting aging.[11] Therefore, we speculated that in the kidneys of 1/6NX and UUO rats, which exhibited the strongest inflammatory reaction, overactivation of PPP increased oxidation reactions and accelerate kidney aging. *In vitro* experiments were also performed to verify our hypothesis.

## Inflammation activates of the PPP in HK-2 cells

To investigate the activation of the PPP induced by inflammation, we examined the expression and activity of G6PD, and the main product-NADPH in HK-2 cells that were cultured in medium containing the inflammatory factors TNF-α or IL-6. The results showed that the expression

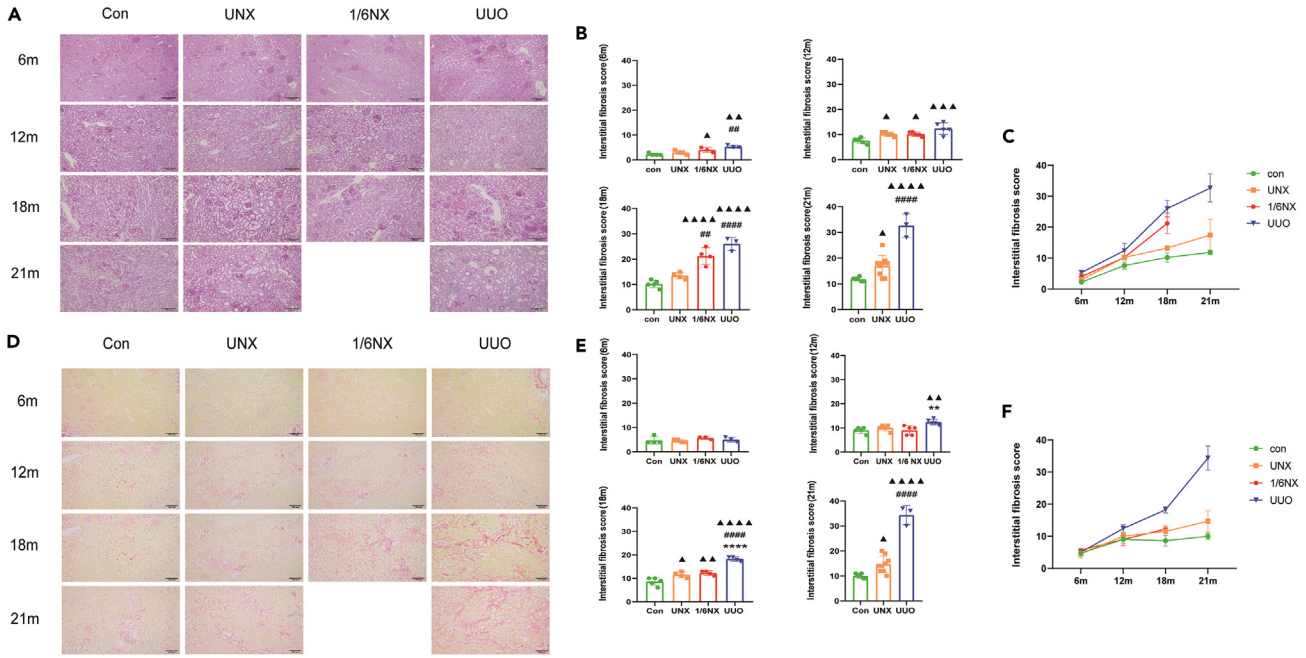


**Figure 4. Renal fibrosis in each group (n = 3–8)**

(A) Periodic acid-Schiff (PAS) staining images of renal tissue at the age of 12,18 and 21 months in each group.

(B) Graph represents the area score of renal interstitial matrix after PAS staining. Scale bars: 100mm.

(C) The trends of renal fibrosis showed by PAS staining with aging.

(D) Sirius red staining images of renal tissue at the age of 12, 18, and 21 months in each group.

(E) Graph represents area score of renal fibrosis after Sirius red staining.

(F) The trends of renal fibrosis showed by Sirius red staining with aging. Data shown as mean ± SD. ▲ $p < 0.05$, ▲▲ $p < 0.01$, ▲▲▲ $p < 0.001$, ▲▲▲▲$p < 0.0001$ versus the control group, ****$p < 0.0001$ versus 1/6NX group, ##$p < 0.01$, ####$p < 0.0001$ versus the UNX group and Sirius red staining of rats in each group.

and activity of G6PD, and NADPH levels were increased by inflammation, indicating activation of the PPP. However, after siG6PD transfection (transfection efficiency is shown in Figure 9A), the overactivation of the PPP was attenuated (Figures 9B–9E).

### Knockdown of G6PD attenuates oxidative stress, aging, and fibrosis in HK-2 cells induced by inflammatory factors

As shown in Figures 10A and 10B, the percentage of SA-β-gal-positive cells significantly increased after 48 h cultured in medium containing inflammatory factor TNF-α or IL-6. Moreover, the expression of aging-related proteins P16, P21, P53, γH2AX, and the expression of COL-I and COL-III were increased notably after 48 h culture (Figures 10C–10I) in medium containing the inflammatory factors TNF-α or IL-6. However, these effects were mitigated by knockdown of G6PD (Figures 10A–10I). Emerging evidence has indicated that overactivation of the PPP, which is a major source of oxidative stress under inflammatory conditions, plays a critical role in progressive tissue and organ injury.[9,10,12] We hypothesized that elevated activity of the PPP increases NADPH production and leads to high levels of oxidative stress and subsequent kidney aging. To test this hypothesis, we determined whether the beneficial effects of knockdown of G6PD were linked to the attenuation of oxidative stress. Our results showed that the increase in ROS, dihydroethidium (DHE), and decrease in T-SOD induced by TNF-α or IL-6 were significantly attenuated by siRNA-mediated G6PD knockdown (Figures 10J–10L).

## DISCUSSION

Senescent or healthy aging kidneys are characterized by nephrosclerosis and the loss of glomerular filtration function, which eventually damages renal function.[4] RFR refers to the difference between the GFR at rest and the maximum volume.[1] Complete renal filtration function includes resting renal function and RFR. In the resting state, the body maintains resting renal function to maintain biological activity, and part of the renal filtration capacity is preserved as RFR. In the stressed state, RFR is released to meet the needs of the body. The resting renal function of nephrons in complete or isolated kidneys is normal, the complete kidney has a normal RFR, RFR is almost lost in isolated kidneys.[13] In this experiment, 1/6 nephrectomy was used to simulate RFR reduction, and UNX was used to simulate the loss of RFR.

Inflammation plays an important role in organ aging. Most aging individuals suffer from inflammatory aging (inflammaging), which is characterized by elevated levels of blood inflammatory markers, which exacerbate cell dysfunction, tissue, and organ failure and body a decline in function.[14] With aging or injury, the accumulation of senescent cells and the development of a senescence-related secretory phenotype

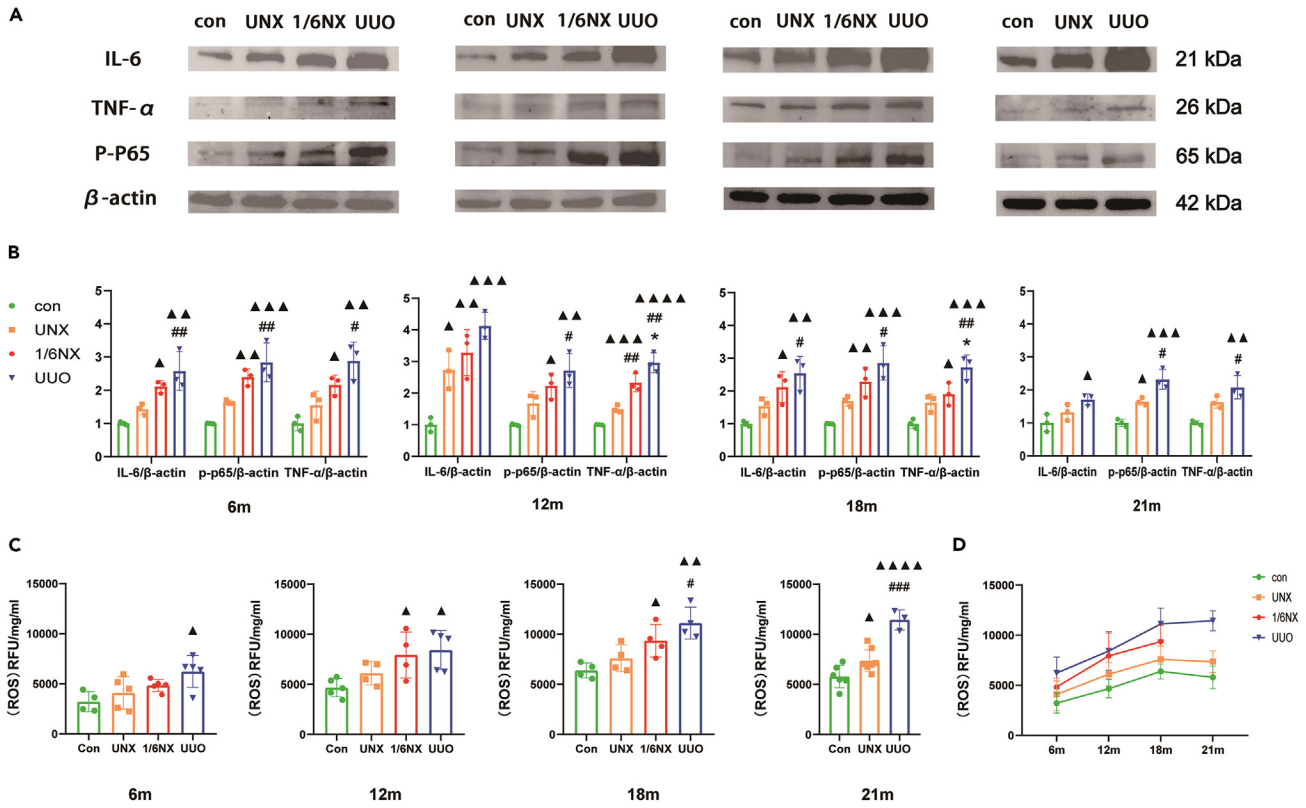


**Figure 5. Renal inflammation and ROS in each group (n = 3–8)**

(A) Protein bands of inflammatory makers IL-6, TNF-α, and p-p65 of renal at the age of 12, 18, and 21 months in each group.

(B) Quantitative analysis results of IL-6, TNF-α, and p-p65.

(C) Renal ROS contents at the age of 12, 18, and 21 months in each group.

(D) The trends of renal ROS content with aging. Data shown as mean ± SD. ▲ $p < 0.05$, ▲▲ $p < 0.01$, ▲▲▲ $p < 0.001$, ▲▲▲▲ $p < 0.0001$ versus the control group, *$p < 0.05$ versus 1/6NX group, #$p < 0.05$, ##$p < 0.01$, ###$p < 0.001$ versus the UNX group.

(SASP) contribute to organ dysfunction.[3,15] A long-term UUO model leads to the loss of renal function on the affected side, and causes persistent kidney inflammation.[16] In this study, the UUO model was used to simulate the coexistence of the loss of renal functional reserve and renal inflammation. Compared with that of young people, the RFR of older adults are significantly decreased.[17] However, it is unknown whether a reduction in RFR can promote kidney aging. Our results showed that compared with that in wild-type rats, UNX, 1/6NX, and UUO rats showed slight trend of fibrosis changes between 6 and 12 months. However, after 18 months, the degree of renal fibrosis in the three models significantly increased after 18 months, and the expression of the aging markers p16, p53, p21, γH2AX, and SA-β-gal content significantly increased. These results suggested that the RFR reduction and renal inflammation could promote kidney aging. Interestingly, compared with wild-type rats, 1/6NX rats showed no obvious changes in kidney weight, kidney volume or cortical thickness. However, the renal inflammatory markers IL-6, TNF-α, p-p65, and renal ROS were significantly increased, and markers of kidney aging and inflammation and the degree of renal interstitial fibrosis were significantly increased compared to those of UNX rats. These results suggested that the role of kidney inflammation in promoting renal aging is stronger than that of RFR reduction. Moreover, the degree of kidney aging in UUO rats with both a decrease in RFR and renal inflammation was the most obvious. These results suggested that the interaction between renal inflammation and RFR reduction could significantly promote kidney aging.

The kidney is an important metabolic organ that not only excludes metabolites, but also participates in the metabolism of carbohydrates, proteins, lipids, and other nutrients.[18] To explore the mechanism through which RFR reduction and renal inflammation influence kidney aging, metabonomic analysis was performed on the unmanipulated kidneys of the three animal models. The results showed that compared with that in wild-type rats, the amino acid metabolism in the kidneys of UNX rats was increased, and the products of several amino acid metabolic pathways were increased, suggesting that RFR reduction affected amino acid metabolism. However, we found that the levels of kynurenate,[19] 3-indoxyl sulfate[20] ethylmalonate,[21] and other tryptophan metabolites, which aggravate renal injury, sarcosine,[22] which has anti-aging properties and is involved in the methionine, glycine, and sarcosine, as well as S-adenosylmethionine (SAM) and its metabolite 5-methylthioadenosine (MTA) which inhibits fibrosis by inhibiting the production of collagen I, reducing lipid peroxidation and reducing oxidative stress, were increased in the UNX group.[22–25] However, which of these amino acid metabolic pathways and their products promote kidney aging and which are the compensatory reactions of the body need further study.

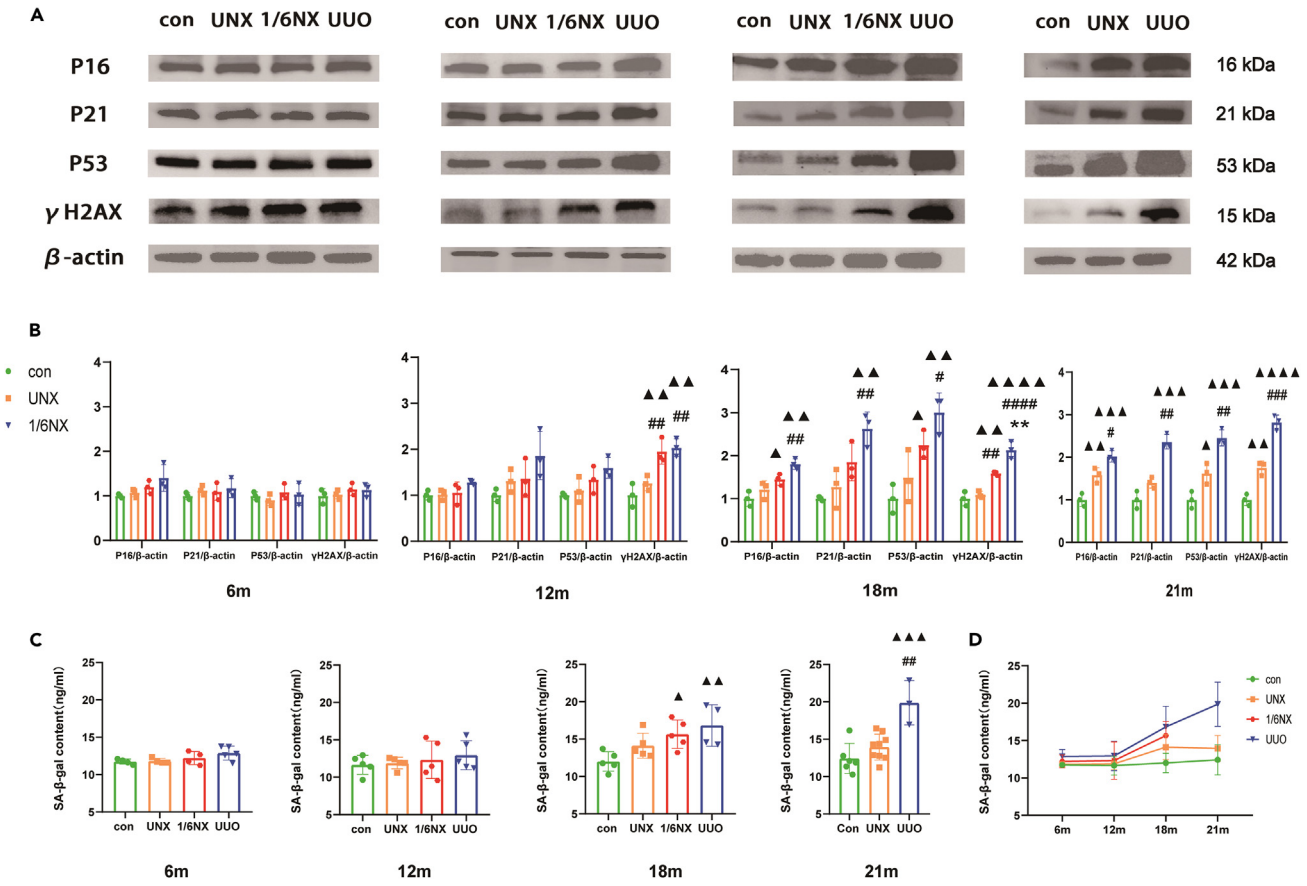


**Figure 6. Renal aging in each group (n = 3–9)**

(A) Protein bands of aging makers P16, P21, P53, and γH2AX of renal at the age of 12, 18, and 21 months in each group.

(B) Quantitative analysis results of P16, P21, P53, and γH2AX.

(C) Renal SA-β-gal content at the age of 12, 18, and 21 months in each group.

(D) The trends of renal SA-β-gal content with aging. Data shown as mean ± SD. ▲ $p < 0.05$, ▲▲ $p < 0.01$, ▲▲▲ $p < 0.001$, ▲▲▲▲ $p < 0.0001$ versus the control group, ** $p < 0.01$ versus 1/6NX group, # $p < 0.05$, ## $p < 0.01$, ### $p < 0.001$, #### $p < 0.0001$ versus the UNX group.

Notably, metabolomics analysis of the 1/6NX and UUO groups showed an increase in PPP metabolites, including 6-phosphogluconate and sedoheptulose-7-phosphate compared to those in wild-type rats, suggesting that the PPP in the kidney was significantly increased in the 1/6NX and UUO models with renal inflammation. Multiple studies have shown that the overexpression of G6PD exerts protective effects on different organs.[26,27] However, under certain inflammatory conditions such as in atherosclerosis, heart failure, and obesity, excessive NADPH due to overactivated G6PD has been shown to promote NADPH oxidase-derived ROS, which may further amplify the inflammatory response.[9,12,28] High glucose-induced activation of the NF-κB signaling pathway promotes the expression of G6PD in adipocytes and activates the PPP, resulting in an enhanced oxidative stress response and further amplification of the inflammatory response.[9] Lipopolysaccharide (LPS) can induce the overexpression of G6PD in microglia[10] and airway epithelial cells[8] to activate the PPP pathway, after which NOX2-mediated oxidative stress and NF-κB are activated, resulting in tissue damage. The connection between oxidative stress and aging has been verified: ROS and redox signals play a critical role in promoting aging[29] and oxidative stress in CKD has been proposed to be the central mechanism that promotes kidney aging, and can lead to muscle consumption and cardiovascular events.[30–32] Moreover, dehydroepiandrosterone (DHEA), which is a noncompetitive G6PD inhibitor, can attenuate aging-related injuries by reducing oxidative stress and the inflammatory response induced by the PPP vivo and *in vitro*.[33] Caloric restriction may protect aging nerves and prolong life by reducing PPP activity.[34] The cerebral cortex of old mice has increased G6PD activity compared with that of young mice, indicating an age-related increase in G6PD activity.[35] By comparing the metabonomics of aging and young human fibroblasts, it was found that aging human fibroblasts have increased PPP activity, glycolysis and gluconeogenesis.[36] Therefore, we hypothesized that the PPP was activated under inflammatory conditions and promoted aging by increasing oxidative stress. We found that inflammation could increase the activation of the PPP, increase the expression and activity of G6PD and increase the production of NADPH in HK-2 cells; PPP over-reactivation was attenuated by siG6PD transfection *in vitro*. Our results also showed that the increase in SA-β-gal, P16, P21, P53, and γH2AX expression levels, and extracellular matrix factors COL-I and COL-III induced by inflammatory factors were significantly attenuated by knockdown of G6PD, indicating that t inhibiting

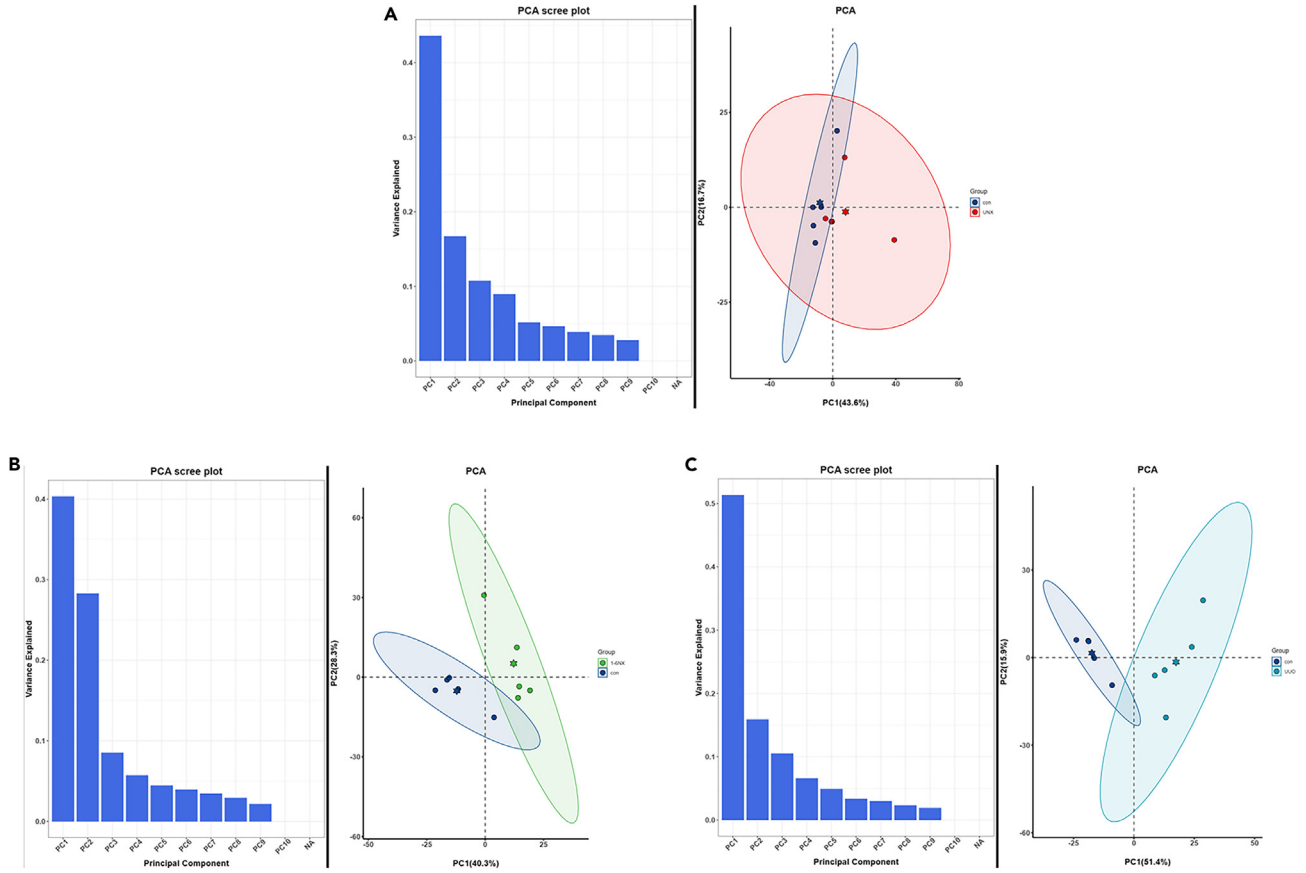


**Figure 7. Untargeted UPLC-MS/MS Analysis-PCA (*n* = 5)**

In the PCA analysis results, the column diagram on the left showed the explanation rate of variance of each principal component, and the distribution of the overall variance on each component could be observed. The scatter diagram on the right showed the projections of samples on first principal component (PC1) and second principal component (PC2). Points of different colors and confidence ellipses indicated different experimental groups. The hexagonal star in the ellipse indicated the central position, and the percentages in parentheses on the horizontal and vertical coordinates indicated the explanation rate of variance of each principal component.

(A) UNX VS control.

(B) 1/6NX VS control.

(C) UUO VS control.

the PPP alleviated the aging and fibrosis induced by inflammation. The response was subsequently activated, as indicated by increased ROS, DHE levels and decreased T-SOD levels after inflammatory stimulation, and oxidative stress was attenuated by inhibiting PPP. Our results further confirmed that inflammation could lead to increased ROS levels and promote renal aging by activating the PPP.

In conclusion, our results indicate that RFR reduction and renal inflammation could accelerate kidney aging, and that the inflammatory state of the kidney plays a major role in this process. Changes in amino acid metabolism caused by RFR reduction and the PPP may also be involved in kidney aging. Our study confirmed that PPP activation leads to increased oxidative stress in HK-2 cells and subsequently accelerates kidney aging. After inhibiting the PPP, the effect of inflammation on cell aging was partially offset. Our study provides the first evidence that RFR reduction promotes kidney aging. It has also been proven that renal inflammation can promote kidney aging caused by RFR reduction. This study provides new ideas for research on the mechanism of kidney aging, and basic evidence for clinical treatment decisions requiring partial or single nephrectomy for kidney inflammation, stones, or tumors.

## Limitations of the study

The initially set sample size was inadequate due to the scarcity of literature reports on the average survival time of surgically treated rats. Consequently, with only 2 rats in the 1/6NX group surviving at 21 months, the data did not provide sufficient statistical power to demonstrate differences. Nonetheless, this observation indirectly underscores the impact of sustained renal inflammation on tissue and organ damage, as well as its role in promoting aging.

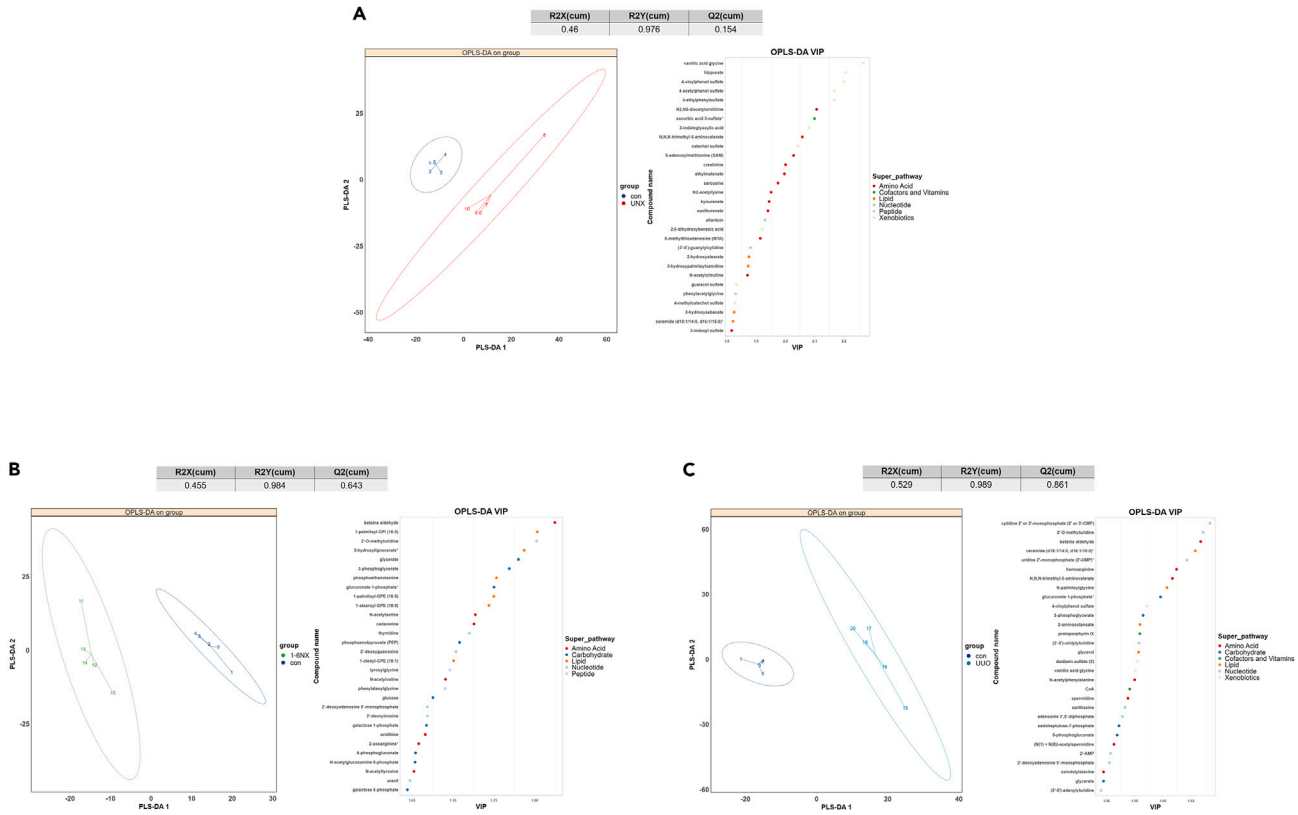


**Figure 8. Projections of samples on the first principal component (PC1) and second principal component (PC2) after PLS-DA analysis (*n* = 5), with different groups identified by different colored ellipses**

In the table, R2X and R2Y represent the explanation rate of variance of PLS-DA model for independent variable matrix and dependent variable matrix, and Q2 represents the prediction ability of PLS-DA model. The right figure was the VIP value of each variable in the PLS-DA model, and the color of the dot indicated the type of the metabolite variable.

(A) UNX VS control.

(B) 1/6NX VS control.

(C) UUO VS control.

## STAR★METHODS

Detailed methods are provided in the online version of this paper and include the following:

- KEY RESOURCES TABLE
- RESOURCE AVAILABILITY
  - Lead contact
  - Materials availability
  - Data and code availability
- EXPERIMENTAL MODEL AND STUDY PARTICIPANT DETAILS
  - Rat
  - Cell lines
- METHOD DETAILS
  - Ultrasound and animal sample preparation
  - Cell transfection and treatment
  - RNA extraction and reverse transcription-polymerase chain reaction (RT-PCR)
  - Renal function studies
  - SA-β-gal assay
  - G6PD activity and NADPH measurement
  - Detection of ROS and T-SOD
  - Histopathologic examination and scoring

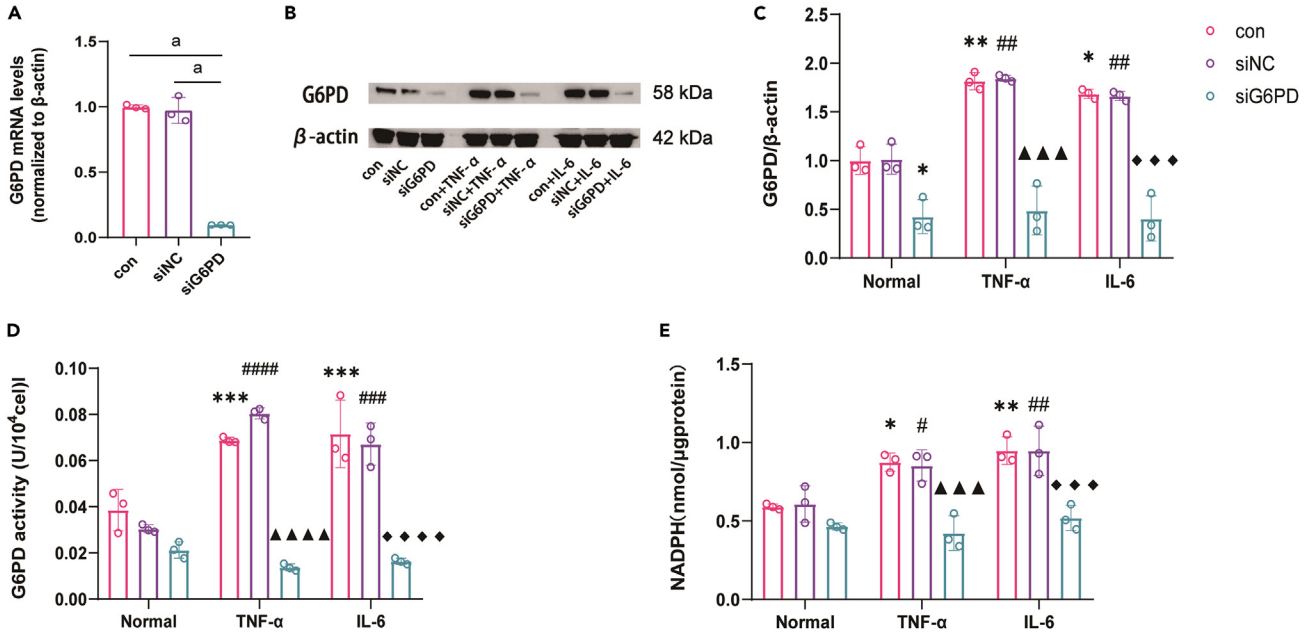


**Figure 9. Inflammation induces the activation of PPP pathway in HK-2 cell (*n* = 3)**

(A) The expression level of G6PD mRNA decreased after being knocked out by siRNA.

(B) Expression of G6PD protein in cells of each group.

(C) Quantitative analysis results of G6PD protein in cells of each group.

(D) Results of G6PD activity in cells of each group.

(E) Results of NADPH content in cells of each group. Data shown as mean ± SD. a < 0.0001，* < 0.05，** < 0.01，*** < 0.001 versus the Normal-control group, # < 0.05, ## < 0.01，### < 0.001，#### < 0.0001 versus the Normal-siNC group，▲▲▲ < 0.001，▲▲▲▲ < 0.0001 versus the TNF-α-control group，◆◆◆ < 0.001 versus the IL-6-control group.

- Western blot
- Untargeted UPLC–MS/MS analysis

- QUANTIFICATION AND STATISTICAL ANALYSIS
  - UPLC–MS/MS
  - *In vivo* and *in vitro* assays

## SUPPLEMENTAL INFORMATION

Supplemental information can be found online at https://doi.org/10.1016/j.isci.2024.110045.

## ACKNOWLEDGMENTS

This work was supported by the National Natural Science Foundation of China (92049103 and 82200780).

## AUTHOR CONTRIBUTIONS

Conceptualization, X.F.S.; methodology, B.H., Y.X.Z., C.L., and P.C.J.; investigation, B.H., Y.X.Z., C.L., P.C.J., Z.H.X., X.D.G., K.C., M.G., Y.Y.L., Y.Z., and Z.N.F.; Visualization, B.H.; writing – original draft, B.H.; writing – eeview & editing, Y.X.Z.; funding acquisition, X.F.S. and C.L.; resources, X.M.C., G.Y.C., X.F.S., and Q.H; supervision, X.M.C., G.Y.C., X.F.S., and Q.H.

## DECLARATION OF INTERESTS

The authors declare no competing interests.

Received: January 17, 2024
Revised: March 20, 2024
Accepted: May 17, 2024
Published: May 22, 2024

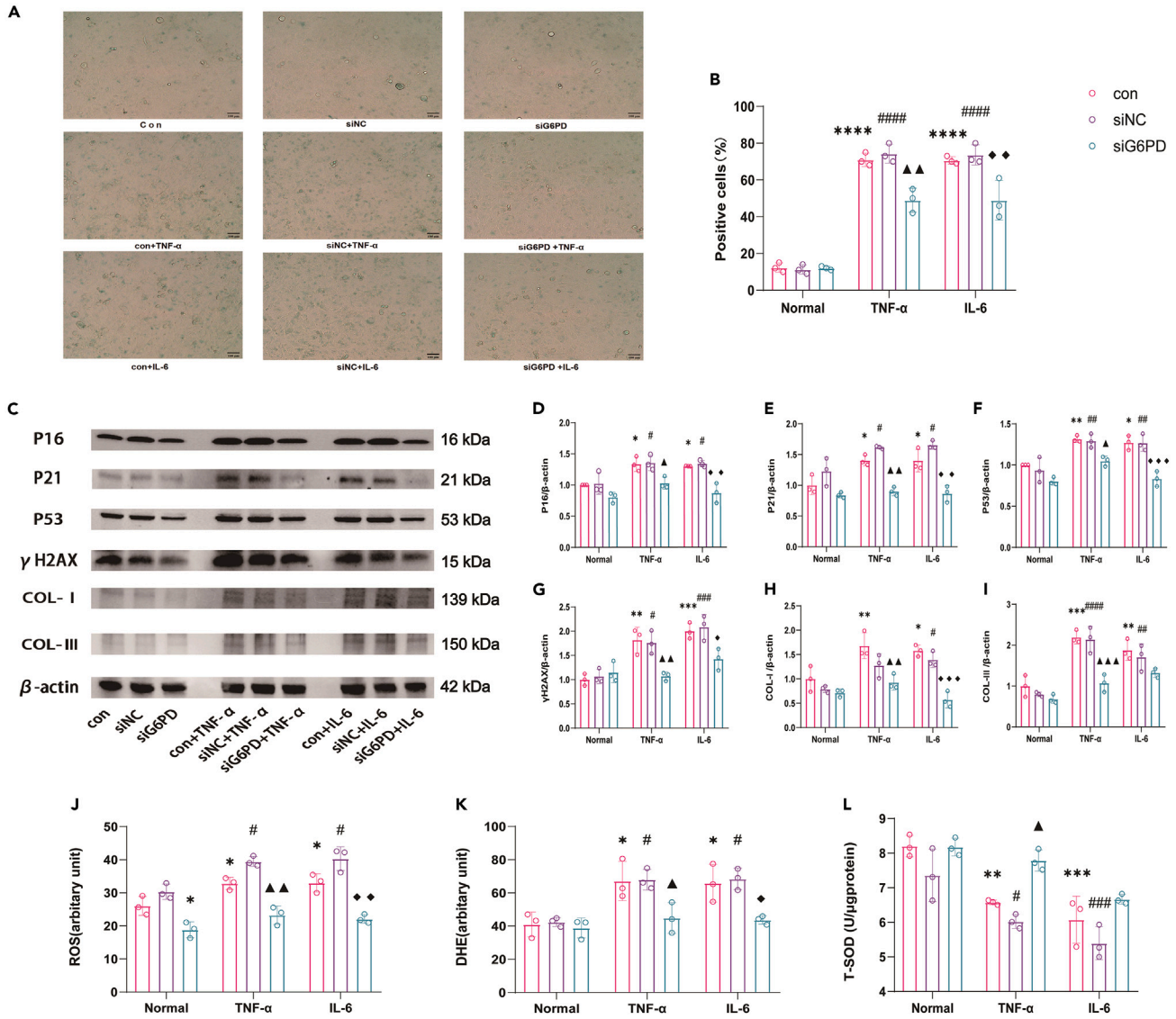


**Figure 10. After the inhibition of PPP pathway, oxidative stress induced by inflammatory factors, cell aging and fibrosis were alleviated (*n* = 3)**

(A) Images of SA-β-galactosidase-positive cells. Scale bars: 100mm.

(B) Positive cell rate statistical results.

(C) Protein bands of P16, P21, P53, γH2AX , COL-I , COL-III of cells of each group.

(D–I) Quantitative analysis results of P16, P21, P53, γH2AX , COL-I , COL-III.

(J) Results of ROS content in cells of each group.

(K) Results of DHE content in cells of each group.

(L) Results of T-SOD content in cells of each group. Data shown as mean ± SD. * < 0.05 , ** < 0.01 , *** < 0.001, **** < 0.0001 versus the Normal-control group, # < 0.05, ## < 0.01 , ### < 0.001 , #### < 0.0001 versus the Normal-siNC group , ▲ < 0.05 , ▲▲ < 0.01 , ▲▲▲ < 0.0001 , versus the TNF-α-control group , ◆ < 0.05, ◆◆ < 0.01 , ◆◆◆ < 0.001 versus the IL-6-control group.

## REFERENCES

1. Palsson, R., and Waikar, S.S. (2018). Renal Functional Reserve Revisited. Adv. Chron. Kidney Dis. *25*, e1–e8. https://doi.org/10.1053/j.ackd.2018.03.001.
2. Orieux, A., Bouchet, A., Doreille, A., Paslaru, L., Livrozet, M., Haymann, J.P., Ouali, N., Mesnard, L., Letavernier, E., and Galichon, P. (2022). Predictive factors of glomerular filtration rate loss associated with living kidney donation: a single-center retrospective study. World J. Urol. *40*, 2161–2168. https://doi.org/10.1007/s00345-022-04019-x.
3. Bridges, C.C., and Zalups, R.K. (2017). The aging kidney and the nephrotoxic effects of mercury. J. Toxicol. Environ. Health B Crit. Rev. *20*, 55–80. https://doi.org/10.1080/10937404.2016.1243501.
4. Denic, A., Glassock, R.J., and Rule, A.D. (2016). Structural and Functional Changes With the Aging Kidney. Adv. Chron. Kidney Dis. *23*, 19–28. https://doi.org/10.1053/j.ackd.2015.08.004.

5. Hodgin, J.B., Bitzer, M., Wickman, L., Afshinnia, F., Wang, S.Q., O'Connor, C., Yang, Y., Meadowbrooke, C., Chowdhury, M., Kikuchi, M., et al. (2015). Glomerular Aging and Focal Global Glomerulosclerosis: A Podometric Perspective. J. Am. Soc. Nephrol. *26*, 3162–3178. https://doi.org/10.1681/ASN.2014080752.
6. Franceschi, C., Garagnani, P., Vitale, G., Capri, M., and Salvioli, S. (2017). Inflammaging and 'Garb-aging'. Trends Endocrinol. Metabol. *28*, 199–212. https://doi.org/10.1016/j.tem.2016.09.005.
7. Mei, C., and Zheng, F. (2009). Chronic inflammation potentiates kidney aging. Semin. Nephrol. *29*, 555–568. https://doi.org/10.1016/j.semnephrol.2009.07.002.
8. Nadeem, A., Al-Harbi, N.O., Ahmad, S.F., Ibrahim, K.E., Siddiqui, N., and Al-Harbi, M.M. (2018). Glucose-6-phosphate dehydrogenase inhibition attenuates acute lung injury through reduction in NADPH oxidase-derived reactive oxygen species. Clin. Exp. Immunol. *191*, 279–287. https://doi.org/10.1111/cei.13097.
9. Park, J., Choe, S.S., Choi, A.H., Kim, K.H., Yoon, M.J., Suganami, T., Ogawa, Y., and Kim, J.B. (2006). Increase in glucose-6-phosphate dehydrogenase in adipocytes stimulates oxidative stress and inflammatory signals. Diabetes *55*, 2939–2949. https://doi.org/10.2337/db05-1570.
10. Tu, D., Gao, Y., Yang, R., Guan, T., Hong, J.S., and Gao, H.M. (2019). The pentose phosphate pathway regulates chronic neuroinflammation and dopaminergic neurodegeneration. J. Neuroinflammation *16*, 255. https://doi.org/10.1186/s12974-019-1659-1.
11. Detienne, G., De Haes, W., Mergan, L., Edwards, S.L., Temmerman, L., and Van Bael, S. (2018). Beyond ROS clearance: Peroxiredoxins in stress signaling and aging. Ageing Res. Rev. *44*, 33–48. https://doi.org/10.1016/j.arr.2018.03.005.
12. Peiro, C., Romacho, T., Azcutia, V., Villalobos, L., Fernandez, E., Bolanos, J.P., Moncada, S., and Sanchez-Ferrer, C.F. (2016). Inflammation, glucose, and vascular cell damage: the role of the pentose phosphate pathway. Cardiovasc. Diabetol. *15*, 82. https://doi.org/10.1186/s12933-016-0397-2.
13. Sharma, A., Mucino, M.J., and Ronco, C. (2014). Renal functional reserve and renal recovery after acute kidney injury. Nephron Clin. Pract. *127*, 94–100. https://doi.org/10.1159/000363721.
14. Ferrucci, L., and Fabbri, E. (2018). Inflammageing: chronic inflammation in ageing, cardiovascular disease, and frailty. Nat. Rev. Cardiol. *15*, 505–522. https://doi.org/10.1038/s41569-018-0064-2.
15. Bolignano, D., Mattace-Raso, F., Sijbrands, E.J.G., and Zoccali, C. (2014). The aging kidney revisited: a systematic review. Ageing Res. Rev. *14*, 65–80. https://doi.org/10.1016/j.arr.2014.02.003.
16. Ucero, A.C., Benito-Martin, A., Izquierdo, M.C., Sanchez-Niño, M.D., Sanz, A.B., Ramos, A.M., Berzal, S., Ruiz-Ortega, M., Egido, J., and Ortiz, A. (2014). Unilateral ureteral obstruction: beyond obstruction. Int. Urol. Nephrol. *46*, 765–776. https://doi.org/10.1007/s11255-013-0520-1.
17. Perschinka, F., Boyer, N., Forni, L.G., and Joannidis, M. (2023). Renal function in very old critically ill patients. Curr. Opin. Crit. Care *29*, 534–541. https://doi.org/10.1097/MCC.0000000000001088.
18. Gewin, L.S. (2021). Sugar or Fat? Renal Tubular Metabolism Reviewed in Health and Disease. Nutrients *13*, 1580. https://doi.org/10.3390/nu13051580.
19. Mor, A., Kalaska, B., and Pawlak, D. (2020). Kynurenine Pathway in Chronic Kidney Disease: What's Old, What's New, and What's Next? Int. J. Tryptophan Res. *13*, 1178646920954882. https://doi.org/10.1177/1178646920954882.
20. Niwa, T., and Shimizu, H. (2012). Indoxyl sulfate induces nephrovascular senescence. J. Ren. Nutr. *22*, 102–106. https://doi.org/10.1053/j.jrn.2011.10.032.
21. Jethva, R., Bennett, M.J., and Vockley, J. (2008). Short-chain acyl-coenzyme A dehydrogenase deficiency. Mol. Genet. Metabol. *95*, 195–200. https://doi.org/10.1016/j.ymgme.2008.09.007.
22. Walters, R.O., Arias, E., Diaz, A., Burgos, E.S., Guan, F., Tiano, S., Mao, K., Green, C.L., Qiu, Y., Shah, H., et al. (2018). Sarcosine Is Uniquely Modulated by Aging and Dietary Restriction in Rodents and Humans. Cell Rep. *25*, 663–676.e6. https://doi.org/10.1016/j.celrep.2018.09.065.
23. Karaa, A., Thompson, K.J., McKillop, I.H., Clemens, M.G., and Schrum, L.W. (2008). S-adenosyl-L-methionine attenuates oxidative stress and hepatic stellate cell activation in an ethanol-LPS-induced fibrotic rat model. Shock *30*, 197–205. https://doi.org/10.1097/shk.0b013e318160f417.
24. Thompson, K.J., Lakner, A.M., Cross, B.W., Tsukada, S., Rippe, R.A., McKillop, I.H., and Schrum, L.W. (2011). S-adenosyl-L-methionine inhibits collagen secretion in hepatic stellate cells via increased ubiquitination. Liver Int. *31*, 891–901. https://doi.org/10.1111/j.1478-3231.2011.02512.x.
25. Nieto, N., and Cederbaum, A.I. (2005). S-adenosylmethionine blocks collagen I production by preventing transforming growth factor-beta induction of the COL1A2 promoter. J. Biol. Chem. *280*, 30963–30974. https://doi.org/10.1074/jbc.M503569200.
26. Serna, E., Mauricio, M.D., San-Miguel, T., Guerra-Ojeda, S., Verdú, D., Valls, A., Arc-Chagnaud, C., De la Rosa, A., and Viña, J. (2023). Glucose 6-P Dehydrogenase Overexpression Improves Aging-Induced Endothelial Dysfunction in Aorta from Mice: Role of Arginase II. Int. J. Mol. Sci. *24*, 3622. https://doi.org/10.3390/ijms24043622.
27. Leopold, J.A., Zhang, Y.Y., Scribner, A.W., Stanton, R.C., and Loscalzo, J. (2003). Glucose-6-phosphate dehydrogenase overexpression decreases endothelial cell oxidant stress and increases bioavailable nitric oxide. Arterioscler. Thromb. Vasc. Biol. *23*, 411–417. https://doi.org/10.1161/01.ATV.0000056744.26901.BA.
28. Gupte, R.S., Floyd, B.C., Kozicky, M., George, S., Ungvari, Z.I., Neito, V., Wolin, M.S., and Gupte, S.A. (2009). Synergistic activation of glucose-6-phosphate dehydrogenase and NAD(P)H oxidase by Src kinase elevates superoxide in type 2 diabetic, Zucker fa/fa, rat liver. Free Radic. Biol. Med. *47*, 219–228. https://doi.org/10.1016/j.freeradbiomed.2009.01.028.
29. Ristow, M. (2014). Unraveling the truth about antioxidants: mitohormesis explains ROS-induced health benefits. Nat. Med. *20*, 709–711. https://doi.org/10.1038/nm.3624.
30. von Haehling, S., Steinbeck, L., Doehner, W., Springer, J., and Anker, S.D. (2013). Muscle wasting in heart failure: An overview. Int. J. Biochem. Cell Biol. *45*, 2257–2265. https://doi.org/10.1016/j.biocel.2013.04.025.
31. Gabai, V.L., Sherman, M.Y., and Yaglom, J.A. (2010). HSP72 depletion suppresses gammaH2AX activation by genotoxic stresses via p53/p21 signaling. Oncogene *29*, 1952–1962. https://doi.org/10.1038/onc.2009.480.
32. Sukhanov, S., Semprun-Prieto, L., Yoshida, T., Michael Tabony, A., Higashi, Y., Galvez, S., and Delafontaine, P. (2011). Angiotensin II, oxidative stress and skeletal muscle wasting. Am. J. Med. Sci. *342*, 143–147. https://doi.org/10.1097/MAJ.0b013e318222e620.
33. Schwartz, A.G., and Pashko, L.L. (2004). Dehydroepiandrosterone, glucose-6-phosphate dehydrogenase, and longevity. Ageing Res. Rev. *3*, 171–187. https://doi.org/10.1016/j.arr.2003.05.001.
34. Yanckello, L.M., Young, L.E.A., Hoffman, J.D., Mohney, R.P., Keaton, M.A., Abner, E., and Lin, A.L. (2019). Caloric Restriction Alters Postprandial Responses of Essential Brain Metabolites in Young Adult Mice. Front. Nutr. *6*, 90. https://doi.org/10.3389/fnut.2019.00090.
35. Bayliak, M.M., Sorochynska, O.M., Kuzniak, O.V., Gospodaryov, D.V., Demianchuk, O.I., Vasylyk, Y.V., Mosiichuk, N.M., Storey, K.B., Garaschuk, O., and Lushchak, V.I. (2021). Middle age as a turning point in mouse cerebral cortex energy and redox metabolism: Modulation by every-other-day fasting. Exp. Gerontol. *145*, 111182. https://doi.org/10.1016/j.exger.2020.111182.
36. James, E.L., Michalek, R.D., Pitiyage, G.N., de Castro, A.M., Vignola, K.S., Jones, J., Mohney, R.P., Karoly, E.D., Prime, S.S., and Parkinson, E.K. (2015). Senescent human fibroblasts show increased glycolysis and redox homeostasis with extracellular metabolomes that overlap with those of irreparable DNA damage, aging, and disease. J. Proteome Res. *14*, 1854–1871. https://doi.org/10.1021/pr501221g.

## STAR★METHODS

### KEY RESOURCES TABLE

| REAGENT or RESOURCE | SOURCE | IDENTIFIER |
|---|---|---|
| Antibodies | | |
| Rabbit monoclonal to P16 | Abcam | ab51243; RRID: AB_2059963 |
| Mouse monoclonal to P21 | Santa Cruz Biotechnology | Cat# sc-6246; RRID: AB_628073 |
| Mouse monoclonal to P53 | Cell Signaling Technology | Cat# 2524; RRID: AB_331743 |
| Rabbit polyclonal to γH2AX | Cell Signaling Technology | Cat# 2577; RRID: AB_2118010 |
| Mouse monoclonal to IL-6 | Santa Cruz Biotechnology | Cat# sc-57315; RRID: AB_2127596 |
| Rabbit monoclonal to p-nuclear factor κB | Cell Signaling Technology | Cat# 3033; RRID: AB_331284 |
| Rabbit polyclonal to TNF-α | Proteintech | Cat# 17590-1-AP; RRID: AB_2271853 |
| Rabbit monoclonal to G6PD | Abcam | Cat# ab133525; RRID:AB_2904024 |
| Rabbit monoclonal to COL-I | Abcam | Cat# ab138492; RRID: AB_2861258 |
| Rabbit monoclonal to COL-III | Abcam | Cat# ab184993; RRID: AB_2895112 |
| Chemicals, peptides, and recombinant proteins | | |
| Recombinant Human TNF-α | Solarbio | P00029 |
| Recombinant Human IL-6 | Solarbio | P00022 |
| Critical commercial assays | | |
| Rat SA-β-gal elisa kit | Jianglaibio | JL54746 |
| Senescence β-Galactosidase Staining Kit | Beyotime Biotechnology | C0602 |
| Glucose 6 phosphate dehydrogenase assay kit | Solarbio | BC0260 |
| NADP/NADPH assay kit | Solarbio | BC 1105 |
| Reactive Oxygen Species Assay Kit | Beyotime Biotechnology | S0033S |
| Tissue reactive oxygen species detection kit | BIO-LAB | HR8820 |
| Dihydroethidium | Beyotime Biotechnology | S0063 |
| Total Superoxide Dismutase Assay Kit | Beyotime Biotechnology | S0101S |
| Liquid chromatography-tandem mass spectrometry (LC-MS/MS) | Calibra Scientific, Inc. | N/A |
| Deposited data | | |
| metabolomics data | N/A | https://www.ebi.ac.uk/metabolights/MTBLS10106 |
| Experimental models: Cell lines | | |
| HK-2 cell | ATCC | CRL-2190 |
| Experimental models: Organisms/strains | | |
| Wistar rats | Experimental Animal Center of General Hospital of PLA | N/A |
| Oligonucleotides | | |
| siRNA targeting sequence: G6PD see Table S1 | Cyagen Biosciences Inc | N/A |
| qRT-PCR primers, see Table S2 | Ji Ma Gene Company | N/A |
| Software and algorithms | | |
| ImageJ | National Institute of health | https://imagej.nih.gov/ij/ |
| GraphPad Prism software | GraphPad | https://www.graphpad.com |

## RESOURCE AVAILABILITY

### Lead contact

Further information and requests for resources and reagents should be directed to and will be fulfilled by the lead contact, Xuefeng Sun (xfssun@126.com).

### Materials availability

This study did not generate new unique reagents.

### Data and code availability

- Metabolomic raw datasets are stored in the Metabolights repository under the entry: MTBLS10106. https://www.ebi.ac.uk/metabolights/MTBLS10106.
- This paper did not generate new codes.
- Any additional information required to reanalyse the data reported in this paper is available from the lead contact upon request.

## EXPERIMENTAL MODEL AND STUDY PARTICIPANT DETAILS

### Rat

The study was approved and by Animal Ethics Committee of the Chinese PLA General Hospital and Military Medical College, approval number [2019-X15-76].

Three-month-old male Wistar rats (180-220g) were provided by the Experimental Animal Center of General Hospital of PLA, and randomly divided into four groups (28 rats in each group): control, unilateral nephrectomy model (UNX), 1/6 nephrectomy model (1/6NX) and unilateral ureteral obstruction model (UUO). Briefly, rats were anesthetized with 60 mg/kg pentobarbital and kept on a heating pad at a temperature of approximately 36.5°C. In the UNX group, a small lumbar incision was made, and the left kidney was removed. Then,1/6 NX was performed by surgical resection of the lower poles (1/3) of the left kidney. In the UUO group, a left laparotomy was performed to expose the left kidney, and the left ureter was isolated through a median abdominal incision and ligated at 2 points with 3–0 silk. Then, the ureter was cut to prevent retrograde infection.

### Cell lines

Human renal tubular epithelial cells (HK-2) were purchased from American Type Culture Collection (ATCC). HK-2 cells were cultured in DMEM/F12 (Gibco, USA) medium supplemented with 10% fetal bovine serum, and in a humidified incubator containing 5% CO2 at 37°C.

## METHOD DETAILS

### Ultrasound and animal sample preparation

The analysis was carried out at the age of 6, 12 and 18 months (n = 5 per group). The remaining rats were all sacrificed at the age of 21 months. The rats were housed in a temperature-controlled environment with a 12-12 h light-dark cycle and maintained with water and food *ad libitum*. At each time-point, renal ultrasound was performed after the rats were anesthetized. Blood was subsequently collected from the abdominal aorta, and the plasma was separated and stored at -80°C used for serum detection. The right kidney tissues were weighed and the ratio of kidney weight to body weight was calculated. Finally, the tissues were cut into two parts: one part was fixed in paraformaldehyde for pathological staining, and the other part was stored in liquid nitrogen for protein detection.

### Cell transfection and treatment

#### *Transfection with siRNA*

SiRNA trageting G6PD (siG6PD) and a negative control (siNC) were transfected into HK-2 cells using Jettime TM (Polyplus-transfection, France) transfection reagent. After 24 hours, the cells were collected for subsequent analysis. The sequences of the siRNAs are shown in Table S1.

#### *Inflammatory factor treatment*

Normal and HK-2 cells transfected with siNC or siG6PD for 24 hours were stimulated with TNF-α (30ng/ml) or IL-6 (30ng/ml) for 48 hours for follow-up observation.

### RNA extraction and reverse transcription-polymerase chain reaction (RT-PCR)

Total RNA was extracted from samples in the different groups using TRIzol reagent according to the manufacturer's protocol (Invitrogen; Thermo Fisher Scientific, Inc.). cDNA was synthesized from the RNA using the SuperScript First-Strand Synthesis system for RT-PCR (Invitrogen; Thermo Fisher Scientific, Inc.). Amplification was performed using FastStart Universal SYBR Green Master Mix (Roche, Germany). The sequences of the primer used are showed in Table S2. Finally, mRNA expression was quantified by the 2ΔΔ CT method and standardized

to β-actin RNA expression. The primers used were designed and synthesized by Ji Ma Gene Company (Jiangsu, China), and the sequences are shown in Table S2.

## Renal function studies

Serum samples were collected and centrifuged at 3000 rpm for 15 minutes and stored at -80°C before analysis. A Hitachi 7150 automatic biochemical analyzer was used to measure rat serum creatinine and urea nitrogen levels.

## SA-β-gal assay

### *Tissue*

The SA-β-gal content in renal tissue was measured using a Rat SA-β-gal elisa kit (Jianglaibio, China). Tissues were washed with PBS, homogenized, and the supernatant was collected. Standards, samples, and an HRP-labeled detection antibody were added to the wells. After a 60-minute incubation at 37°C, the plate was washed, substrates A and B were added, and incubated for 15 minutes at 37°C in the dark. OD values were then measured at 450nm. Normalize the values to total protein levels in cell lysates determined using a bicinchoninic acid (BCA) protein assay.

### *Cell*

Cellular SA-β-gal activity was assessed using the Senescence assay kit (Beyotime Biotechnology, China) following the provided guidelines. Cells were fixed for 15 minutes and then stained with the Staining Mixture at 37°C without CO2 overnight. SA-β-gal-positive cells, appearing blue, were imaged randomly. The percentage of senescent HK-2 cells was determined from five different fields of view. The experiments were conducted at least three times.

## G6PD activity and NADPH measurement

The activity of G6PD and the level of NADPH in cultured cells were measured according to the manufacturer's instructions using glucose 6 phosphate dehydrogenase assay kit (Solarbio, China) and an NADP/NADPH assay kit (Solarbio, China), respectively.

## Detection of ROS and T-SOD

### *ROS of tissue*

Take a 50mg tissue sample, rinse with PBS, and homogenize in 1ml of buffer. Collect the supernatant. Mix 190μl of supernatant with 10μl of O12 probe in a 96-well plate, mix thoroughly, and incubate at 37°C in the dark for 30 minutes. Measure fluorescence intensity at 488nm excitation and 530nm emission. Normalize the values to total protein levels in cell lysates determined using a bicinchoninic acid (BCA) protein assay.

### *ROS of cell*

The production of intracellular ROS (iROS) was measured by the fluorescence probe chloromethyl-29, 79-dichlorodihydrofluorescein diacetate (CM-H2DCFDA; Beyotime Biotechnology, China). Briefly, cells cultured in 6-well plates were transfected with vehicle, siNC or G6PD for 24 h followed by treatment with TNF-α or IL-6 for 48 h. After the cells were incubated with H2DCFDA (106 cell/ml) for 20 min at 37°C, the fluorescence intensity was mresured at an excitation wavelehgth of 488 nm and an emission wavelehgth of 525 nm using Spark multifunctional enzyme label instrument (Tecan, Switzerland).

### *Dihydroethidium (DHE) of Cell*

Cells from a six-well plate were collected and homogenized. They were incubated with 0.5μM Dihydroethidium at 37°C for 30 minutes, washed, and then fluorescence was measured using an enzyme-labeled instrument with 300nm excitation and 610nm emission.

### *T-SOD of Cell*

Cell total SOD levels in the different groups were determined according to the instructions of the T-SOD assay kit (Beyotime Biotechnology, China), and the levels of T-SOD were determined by measuring the absorbance at 450 nm.

## Histopathologic examination and scoring

Paraformaldehyde-fixed renal tissues were embedded in paraffin. Three-micrometer sections were cut from the tissue blocks and stained with Sirius red to assess fibrosis. Under an optical microscope, 10 rendom fields of view were selected from each section under an optical microscope to determine the extent of fibrosis based on the following scoring system: 0% was counted as 0 point, 0%-25% was counted as 1 point, 25%-50% was counted as 2 points, 50%-75% was counted as 3 points, > 75% was counted as 4 points.

Periodic Acid-Schiff staining was used for the semiquantitative scoring of tubulointerstitial lesions, focusing on tubular atrophy, interstitial inflammatory cell infiltration, and interstitial fibrosis. Ten nonoverlapping fields at a 100× magnification were captured and average scores were calculated. Scoring was based on the percentage of lesions in the renal interstinal area: 0 % was counted as 0 point, 0%-25% was counted

as 1 point, 25%-50% was counted as 2 points, 50%-75% was counted as 3 points, > 75% was counted as 4 points. Two masked investigators assigned histologic scores. Ten randomly chosen, nonoverlapping fields per animal wereassess for accurate evaluation.

### Western blot

Renal tissues or collected cells were homogenized in lysis buffer containing protease and phosphatase inhibitors, and the protein concentration was measured using the bicinchoninic acid protein assay (Thermo Fisher Scientific, USA). The samples were then separated on 8%-10% SDS-polyacrylamide gels (PAGE) and transferred onto nitrocellulose membranes. After being blocked with 1×CASEIN, the membranes were incubated with the following primary antibodies overnight at 4°C: β-actin (20536-AP, Proteintech), P16 (ab51243, Abcam), P21 (sc-6246, Santa Cruz Biotechnology), P53 (2524, Cell Signaling Technology), γH2AX (2577, Cell Signaling Technology) , IL-6 (sc-57315, Santa Cruz Biotechnology), p-nuclear factor κB (3033, Cell Signaling Technology) and TNF-α (17590-1-AP, Proteintech), G6PD (ab133525, Abcam), COL-I (138492, Abcam), and COL-III (184993, Abcam). The blots were probed with HRP-conjugated secondary antibodies (Beyotime) for 2 h at room temperature. Immunoreactive bands were visualized by enhanced chemiluminescence, and the intensities were measured using ImageJ software (Scion Corporation).

### Untargeted UPLC–MS/MS analysis

Untargeted metabolomic analysis was conducted by Calibra Lab at DIAN Diagnostics (Hangzhou, Zhejiang, China) on their CalOmics metabolomics platform. Samples were homogenized and extracted using methanol in a ratio of 1:4. The mixtures were shaken for 3 minutes and precipitated by centrifugation at 4000× g, 10 minutes at 20°C. Four aliquots of 100 μL supernatant were transferred to sample plates and dried under blowing nitrogen, then re-dissolved in reconstitution solutions for sample injection into UPLC-MS/MS systems. The instruments for the four UPLC-MS/MS methods are ACQUITY 2D UPLC (Waters, Milford, MA, USA) plus Q Exactive (QE) hybrid Quadrupole-Orbitrap mass spectrometer (Thermo Fisher Scientific, San Jose, USA). QE mass spectrometer was operated at a mass resolution of 35000, the scan range was 70-1000 m/z. In the first UPLC-MS/MS method, QE was operated in positive ESI mode and the UPLC column was C18 reverse-phase (UPLC BEH C18, 2.1x100 mm, 1.7 um; Waters); the mobile solutions used in the gradient elution were water (A) and methanol (B) containing 0.05% PFPA and 0.1% FA. In the second UPLC-MS/MS method, QE was operated in negative ESI mode, and the UPLC column was C18 reverse-phase (UPLC BEH C18, 2.1x100 mm, 1.7 um; Waters), the mobile solutions used in the gradient elution were water (A) and methanol (B) containing 6.5 mM ammonium bicarbonate at pH 8. The third UPLC-MS/MS method had the QE operated in ESI positive mode and the UPLC column was C18 reverse-phase (UPLC BEH C18, 2.1x100 mm, 1.7 um; Waters), the mobile solutions were water (A) and methanol/acetonitrile/water (B) contain 0.05% PFPA and 0.01% FA. In the fourth method, QE was operated in negative ESI mode, the UPLC column was HILIC (UPLC BEH Amide, 2.1x150 mm, 1.7 um; Waters), and the mobile solutions were water (A) and acetonitrile (B) with 10 mM ammonium formate.

## QUANTIFICATION AND STATISTICAL ANALYSIS

### UPLC–MS/MS

All metabonomics statistical analyses were performed with R language (R version 3.4.1: http://www.cran.com; Rstudio version 1.4.1717 https://www.rstudio.com; mixOmics version 6.10.9 http://mixomics.org/. Multivariate analysis approaches including principal component analysis (PCA), partial least square discriminate analysis (PLS-DA) were conducted. When there are only two sample groups, orthogonal partial least square discriminant analysis (OPLS-DA) would be used instead of PLS-DA. Result visualization were provided for the performed statistical analyses, including volcano plot in differential metabolite test, scatter plot with confidence ellipse in PCA, scatter plot with confidence ellipse and variable importance dot plot in PLS-DA/OPLS-DA.

### *In vivo* and *in vitro* assays

The data examined are expressed as the means ± standard deviations (SDs). Statistical analysis was performed using GraphPad Prism software (La Jolla, CA). Comparisons between groups were made using one-way ANOVA followed by the Student-Newman-Kuels test. $P<0.05$ was considered to indicate statistical significant. All error bars indicate the SD of mean. Sample sizes and any additional statistical details can be found in the figure legends.